Computers and Geotechnics 132 (2021) 104017

Contents lists available at ScienceDirect

Computers and Geotechnics

journal homepage: www.elsevier.com/locate/compgeo

Research Paper

# Seismic stability of coal tailings dams with spatially variable and liquefiable coal tailings using pore pressure plasticity models

Sajjad Salam [a,*], Ming Xiao [b], Arash Khosravifar [c], Katerina Ziotopoulou [d]

[a] Exponent, 525 W Monroe St STE 1050, Chicago, IL 60661, United States
[b] Department of Civil and Environmental Engineering, The Pennsylvania State University, University Park, PA 16802, United States
[c] Department of Civil and Environmental Engineering, Portland State University, Portland, OR 97201, United States
[d] Department of Civil and Environmental Engineering, University of California, Davis, CA 95616, United States

ARTICLE INFO

*Keywords:*
Coal tailings
Liquefaction behavior
Tailings dams
Seismic stability
Stochastic modeling
PM4Silt

ABSTRACT

Failure of tailings dams can result in significant spill, loss of human lives, and damages to the environment and infrastructure. Cyclic loadings such as earthquakes and blasting are among the main threats to the stability of tailings dams. Seismic stability analyses of tailings dams are further challenged by the uncertainty and variability of tailings properties. In this paper, the influence of input motion characteristics and spatial variability in coal tailings (CT) properties on the seismic stability of a typical upstream-construction CT dam is investigated. Among the input motion characteristics, peak ground acceleration (PGA), equivalent number of cycles (ENC), and frequency content are the focus of this study. First, the applicability of two advanced constitutive plasticity models, PM4Sand and PM4Silt, in simulating the cyclic behavior of CT is evaluated and a suitable model is selected. The undrained shear strength of CT is modeled as a spatially correlated Gaussian random field. Six input motions — one blast and five earthquakes — are selected for the dynamic analyses. The dynamic analyses are conducted in co-seismic and then post-seismic stages. The seismic stability of the CT dam with uniform properties (i.e. uniform models) is compared to the stochastic models under the selected input motions. Post-seismic analysis was found critical for the stochastic models. This study highlights the importance of stochastic modeling and the consideration of spatial variability in seismic stability analysis of CT dams.

## 1. Introduction

Coal tailings (CT) are the residue as a result of mine extraction process and mostly consist of water, coal fraction, and non-coal materials such as sand and silt. CT are commonly characterized as low plasticity silty sand to sandy silt and are typically deposited in the form of slurry behind tailings dams. Generally, tailings dams have more vulnerability than conventional and engineered dams used for water storage, and their annual failure rate is 120 times higher than that of water-storage dams (Azam and Li, 2010). Tailings dams are constructed by three methods: downstream, centerline, and upstream, and the upstream configuration has the least stability (Vick, 1990; Rico et al., 2008). A recent example of a tailings dam failure was the Vale's Brumadinho iron ore tailings dam in Brazil in 2019, which was the 11th most serious tailings dam failure in the last decade and resulted in over 300 life losses and significant social, economic, and environmental impacts (Home, 2019).

One of the most common causes of tailings dams' failure is liquefaction (ICOLD, 2001; Plant and Harriman, 2008). Liquefaction of CT could lead to different forms of failure such as failure of the dam's slope due to weakened and liquefied underlying layers, overtopping of the liquefied material, and increase of lateral pressure on the dikes (ICOLD, 2001). Engineering procedures and numerical modeling tools can be used to better approximate these complex processes and consequently assess the seismic stability of CT dams for a variety of demand and capacity scenarios. Various constitutive plasticity models such as UBCSAND (Beaty and Byrne, 1998), PM4Sand (Boulanger and Ziotopoulou, 2017), and PM4Silt (Boulanger and Ziotopoulou, 2018) have been developed to approximate the response of sand and low plasticity silt in earthquake engineering applications. However, the applicability of these models to simulate cyclic behavior of CT has not been accurately assessed. UBCSAND, a non-linear effective stress plasticity model, was proposed by Beaty and Byrne (Beaty and Byrne, 1998) to determine the

* Corresponding author.
*E-mail addresses:* ssalam@exponent.com (S. Salam), mxiao@engr.psu.edu (M. Xiao), karash@pdx.edu (A. Khosravifar), kziotopoulou@ucdavis.edu (K. Ziotopoulou).

https://doi.org/10.1016/j.compgeo.2021.104017
Received 21 July 2020; Received in revised form 3 December 2020; Accepted 17 January 2021

mechanical response of sand under cyclic loading. UBCSAND has been used to simulate the dynamic behavior of sand and low plasticity tailings in engineering practices (Castillo et al., 2005; Ferdosi et al., 2015; James, 2009; Seid-Karbasi and Byrne, 2004). PM4Sand and PM4Silt are plane-strain bounding-surface plasticity models developed by Boulanger and Ziotopoulou (Boulanger and Ziotopoulou, 2017; Boulanger and Ziotopoulou, 2018). PM4Sand assesses the drained and undrained, and cyclic and monotonic mechanical responses of sands and non-plastic silts, while PM4Silt assesses those of low plasticity silts and clays. Both the PM4Sand and PM4Silt plasticity models are based on the framework of the stress-ratio controlled, critical state compatible, bounding-surface plasticity model for sand developed by Dafalias and Manzari (Dafalias and Manzari, 2004). PM4Sand and PM4Silt have been successfully used to simulate both sandy materials (Ziotopoulou and Montgomery, 2017; Ziotopoulou and Boulanger, 2016) and alluvial silty deposits (Boulanger et al., 2019; Boulanger, 2019; Boulanger and Montgomery, 2016). Field and laboratory testing by Salam et al. (Salam et al., 2019) showed that the cyclic behavior of CT is complex and transitions from sand-like to clay-like, because the composition of CT is a mixture of sand and silt. Therefore, both PM4Sand and PM4Silt could be potentially used for simulating the cyclic behavior of CT.

Coal tailings have noticeable heterogeneity and spatial variability. In a recent study, Liew et al. (Liew et al., 2020) showed the significant heterogeneity in coal tailings properties using in-situ seismic investigations in an active Appalachian coalfield. Such spatial variability of slurry's geotechnical properties is caused by variations of slurry discharge locations and extracted coal materials during the service time of a tailings impoundment. Therefore, the spatial variability of properties should be considered in the stability analyses, as a model with uniform properties may not capture the critical failure modes. For example, the failure of the Kingston Tennessee Valley Authority (TVA) coal ash impoundment was partially due to the liquefaction of a loose layer under the dikes (Plant and Harriman, 2008). This mode of failure cannot be estimated unless the stratified medium of tailings is accounted for in the stability analysis.

In this paper, the uncertainty in seismic response of a typical upstream-construction CT dam is analyzed considering the variability in CT geotechnical properties. A suitable pore pressure plasticity model for simulating the cyclic response of CT is selected through single element simulations and calibrations against experimental results. A representative number of realizations for the CT section of the dam are generated by the Karhunen-Loeve expansion method. It is of interest to evaluate how system response and its uncertainty are influenced by input motion characteristics such as peak ground acceleration (PGA), equivalent number of cycles (ENC) as a proxy for duration, and frequency content. Six input motions representing a variety of PGA, ENC, and frequency content are selected for the numerical simulations. The seismic performance of the CT dam is analyzed under co-seismic stage and then post-seismic stage to consider the volumetric strains due to reconsolidation after each shaking event. Uniform models are also studied and compared to the stochastic models to illustrate the necessity of stochastic modeling.

## 2. Model configuration

A typical upstream-construction CT dam was generated in the Fast Lagrangian Analysis of Continua (FLAC Version 8) commercial platform, as shown in Fig. 1. The geometry approximately followed the geometry of Mochikochi tailings dam, discussed in Byrne and Seid-Karbasi (Seid-Karbasi and Byrne, 2004). As reported by Rico et al. (Plant and Harriman, 2008), 45% of failed tailings dams had height less than 15 m. Accordingly, the generated model was 90 m long and 15 m tall including a 3-m thick bedrock and 12-m thick CT behind a 3:1 (H:V) slope formed by four dikes, each 3 m high. The model was made long enough such that the failure mechanism around the slope is not influenced by the boundaries. The meshing was implemented such that the spatial element size was small, particularly in the vertical direction, to ensure proper wave transmission through the model (Itasca Consulting Group, 2017).

The dikes and bedrock properties were adopted from studies where the cyclic behavior and seismic stability of CT dams were evaluated. The bedrock was assumed to be an elastic and homogeneous material with a density of 2400 kg/m$^3$, a shear modulus of 860 MPa, and a Poisson's ratio of 0.3 in all simulations. The dikes, which are typically constructed with gravelly sand, were modeled using the Mohr-Coulomb elastoplastic model. The density, cohesion, and friction angle of the dikes were selected to be 1700 kg/m$^3$, 10 kPa, and 35°, respectively, based on previous studies (Byrne and Seid-Karbasi, 2003; Ferdosi et al., 2015; Zeng et al., 2008). The shear modulus of the dikes was pressure-dependent with Poisson's ratio of 0.3 and calculated based on the Hardin (Hardin, 1978) equation that was developed for granular materials. The default hysteresis model in FLAC2D was used among the built-in tangent modulus functions to define the shear modulus reduction curves for the dikes (Itasca Consulting Group, 2017). The input parameters for the default hysteresis model were adopted from Zeng et al. (Zeng et al., 2008).

The spatial variability in geotechnical properties of CT is significant mainly due to the depositional processes in the field. A uniform model for the CT may not accurately represent the system response under loading events. In this study, CT were studied as uniform and spatially variable materials, respectively. Since CT are composed of sand and low plasticity silt and demonstrate cyclic behaviors that could be interpreted as either cyclic liquefaction or cyclic mobility, both PM4Sand and PM4Silt could be considered in the design and analysis. The applicability and calibration of both models for the CT are presented in the next section.

The hydrostatic pore pressure was established through the model, and the CT were assumed to be fully saturated and the toe of the bottom dike was the drainage zone. The boundaries were extended sufficiently far from the failure zone to minimize the influence of boundaries on the model response. A free-field boundary condition was assigned to the side boundaries and a quiet boundary was considered at the bottom boundary in both the horizontal and vertical directions during the dynamic analyses. The outcrop input motions were applied in a form of shear stress time series at the base of the model using the compliant-base procedure by Mejia and Dawson (Mejia and Dawson, 2006). A Rayleigh

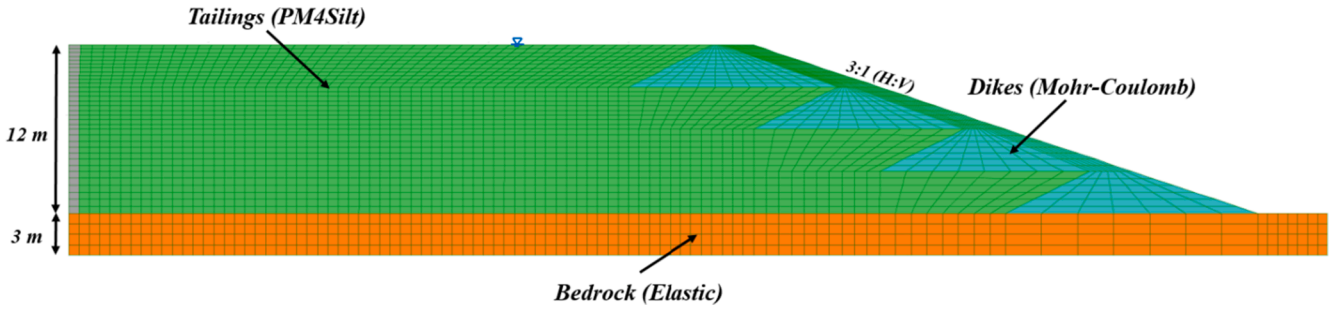


**Fig. 1.** Typical upstream-construction CT dam model generated in FLAC2D.

damping of 0.5% at a center frequency of 3 Hz was considered for the CT to account for low-strain damping (Boulanger and Montgomery, 2016). Only the CT were considered liquefiable and water flow was not permitted during the dynamic analyses due to the low permeability of CT (Salam et al., 2019). The average permeability of the CT studied by Salam et al. (Salam et al., 2019) was $6 \times 10^{-6}$ cm/s, which justifies the undrained condition assumption under cyclic loading. The first column of the zones at the far left boundary was considered non-liquefiable to avoid inaccurate free-field boundary calculations, as recommended by the FLAC2D manual (Itasca Consulting Group, 2017).

The seismic performance of the CT dam was evaluated in two stages: 1) during the cyclic loading (i.e. co-seismic) and 2) after the cyclic loading (i.e. post-seismic). Co-seismic analysis included the non-linear effective stress analysis during the motion. Post-seismic analysis considered the excess pore pressure dissipation and effective stress increase after the motion. Accordingly, the dynamic analysis was continued after each shake to determine the volumetric strains due to reconsolidation. An empirical approach of reducing elastic shear modulus was used in PM4Sand and PM4Silt to calculate the volumetric strains during the reconsolidation process (Boulanger and Ziotopoulou, 2017; Boulanger and Ziotopoulou, 2018).

### 2.1. PM4Sand and PM4Silt calibration based on CT cyclic response

Both PM4Sand and PM4Silt models require three primary input parameters. The contraction rate parameter ($h_{po}$), which estimates the plastic volumetric strain rate, is the first primary input parameter and is required in both models. $h_{po}$ is a soil specific input parameter and should be calibrated based on the relationship of cyclic stress ratio (CSR) versus the number of cycles (N) to reach liquefaction, i.e., the CSR-N curve determined by laboratory testing. Shear modulus coefficient, $G_0$, is the second primary input parameter and is required in both models. The elastic shear modulus is determined by $G_0$. The remaining primary input parameters, relative density ($D_r$) for PM4Sand, and undrained shear strength at critical state under earthquake loading ($s_{u,cs,eq}$) for PM4Silt, are determined by either empirical relationships or in-situ and laboratory tests. Undrained shear strength ratio ($s_{u,cs,eq\_Rat}$), which is $s_{u,cs,eq}$ normalized by vertical effective stress, is used in this study instead of $s_{u,cs,eq}$. In addition to the primary input parameters, there are eighteen and twenty secondary input parameters defined in the PM4Sand and PM4Silt models, respectively.

To evaluate the applicability of PM4Sand and PM4Silt in simulating the cyclic behavior of CT, the cyclic response of anthracite CT in cyclic direct simple shear (cyclic DSS) tests reported by Salam et al. (Salam et al., 2019) was simulated by both models. The CT showed a transitional cyclic behavior from clay-like to sand-like in Salam et al. (Salam et al., 2019). Accordingly, either cyclic liquefaction or cyclic mobility is likely to be observed in CT during cyclic loading. This characteristic is due to the composition of CT (i.e. mixture of sand and silt) and plasticity index less than or equal to 7 (Salam et al., 2019). Therefore, it is necessary to examine the abilities of both PM4Sand and PM4Silt in capturing the cyclic behavior of CT.

Based on the available experimental data, only primary input parameters were used to calibrate the models for the tested CT; the secondary input parameters retained their default values. Thus, the experimental CSR-N curve was not closely matched by the model simulations. This approach is in line with the model application in the practice, where oftentimes data are only available to calibrate primary input parameters. The primary input parameters, $D_r$, $s_{u,cs,eq\_Rat}$, and $G_o$ of the CT sample in Salam et al. (Salam et al., 2019) were 50%, 0.25, and 160, respectively. The contraction rate parameter, $h_{po}$, was calibrated for both models to match the CSR determined using cyclic DSS tests at 15 cycles. The effective vertical stress in the cyclic DSS tests and the numerical calibration was 60 kPa. Using single element simulations, the $h_{po}$ parameter was calibrated for CT to a value of 0.21 and 0.83 in PM4Sand and PM4Silt, respectively. The CSR-N curve on log-scale can be expressed by a power law of $CSR = a \times (N_{failure})^{-b}$, where $N_{failure}$ is defined as number of cycles to reach 5% double amplitude shear strain (DAS) in the cyclic DSS tests. The experimental and simulated CSR-N curves and the corresponding equations are shown in Fig. 2. The estimated $b$-value in the PM4Sand and PM4Silt simulations was 0.25 and 0.23, respectively, while the $b$-value from the cyclic DSS test was 0.17. The CSR-N curves in Fig. 2 show that both PM4Sand and PM4Silt performed similarly in estimating the liquefaction resistance of the CT. Both models approximated higher cyclic resistance at large CSR values compared to the cyclic DSS test results. For example, the simulated CT reached failure at larger number of cycles at CSR of 0.15 compared to the cyclic DSS test result. To further investigate the applicability of PM4Sand and PM4Silt in approximating the cyclic response of the CT, the shear stress-strain loops, shear strain accumulation, and pore pressure ratio from the experiments and the simulations were compared.

The simulated stress-strain loops by PM4Sand and PM4Silt are compared against the cyclic DSS test results and are shown in Fig. 3 (a) and (b) for CSR of 0.12. According to Fig. 3 (a) and (b), although the initial plastic behavior of CT was not captured by the models, the wide shear stress-strain loops that were observed through cyclic loading were better approximated by PM4Silt than by PM4Sand. However, both models estimated the 5% DAS occurrence at comparable number of cycles (i.e. $N \approx 10$). Fig. 3 (c) and (d) show the accumulation of shear strain with number of cycles approximated by PM4Sand and PM4Silt. The soil element simulated by PM4Sand did not accumulate large shear strains until the last cycle, where the sample suddenly reached 5% DAS. The soil element simulated by PM4Silt experienced progressive accumulation of shear strain until failure, similar to the laboratory observation. In addition, the excess pore pressure ratios ($r_u$) estimated by PM4Sand and PM4Silt along with the observed $r_u$ in the cyclic DSS test are shown in Fig. 3 (e) and (f). The difference in estimating excess pore pressure ratio by PM4Sand and PM4Silt was small since the final $r_u$ was approximated as 0.8 ~ 0.9 by both PM4Sand and PM4Silt. The estimated $r_u$ by PM4Sand was found to approximate the lower bound of $r_u$ from cyclic DSS test before the last cycle, as shown in Fig. 3 (e). According to Fig. 3 (f), the trend of pore pressure ratio with the cycles was slightly better approximated by the PM4Silt model. The transitional behavior of CT between clay-like and sand-like behavior observed by Salam et al. (Salam et al., 2019) was further confirmed by noticing insignificant differences between PM4Sand and PM4Silt calibration results. Both models showed limitations in approximating the cyclic behavior of the tested sample such as higher resistance at high CSRs and the initial elastic behavior under cyclic loading. Overall, PM4Silt showed better approximation specifically in terms of strain accumulation and cyclic mobility (i.e. softening) of the CT. In addition to the calibration results, a shear strength related index ($S_{u,cs,eq\_Rat}$ in PM4Silt)

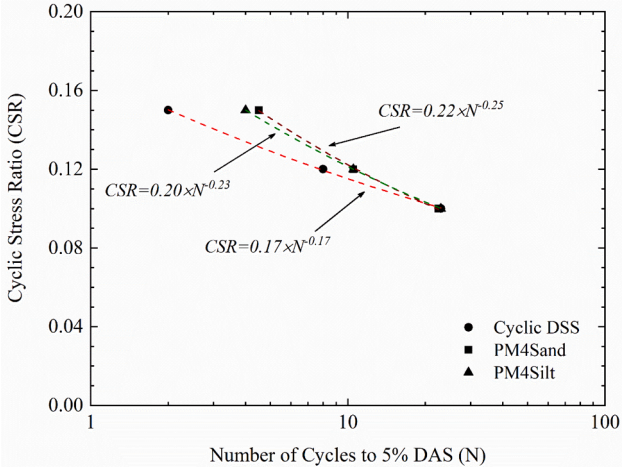


**Fig. 2.** Experimental and numerically simulated CSR-N curves for the studied CT.

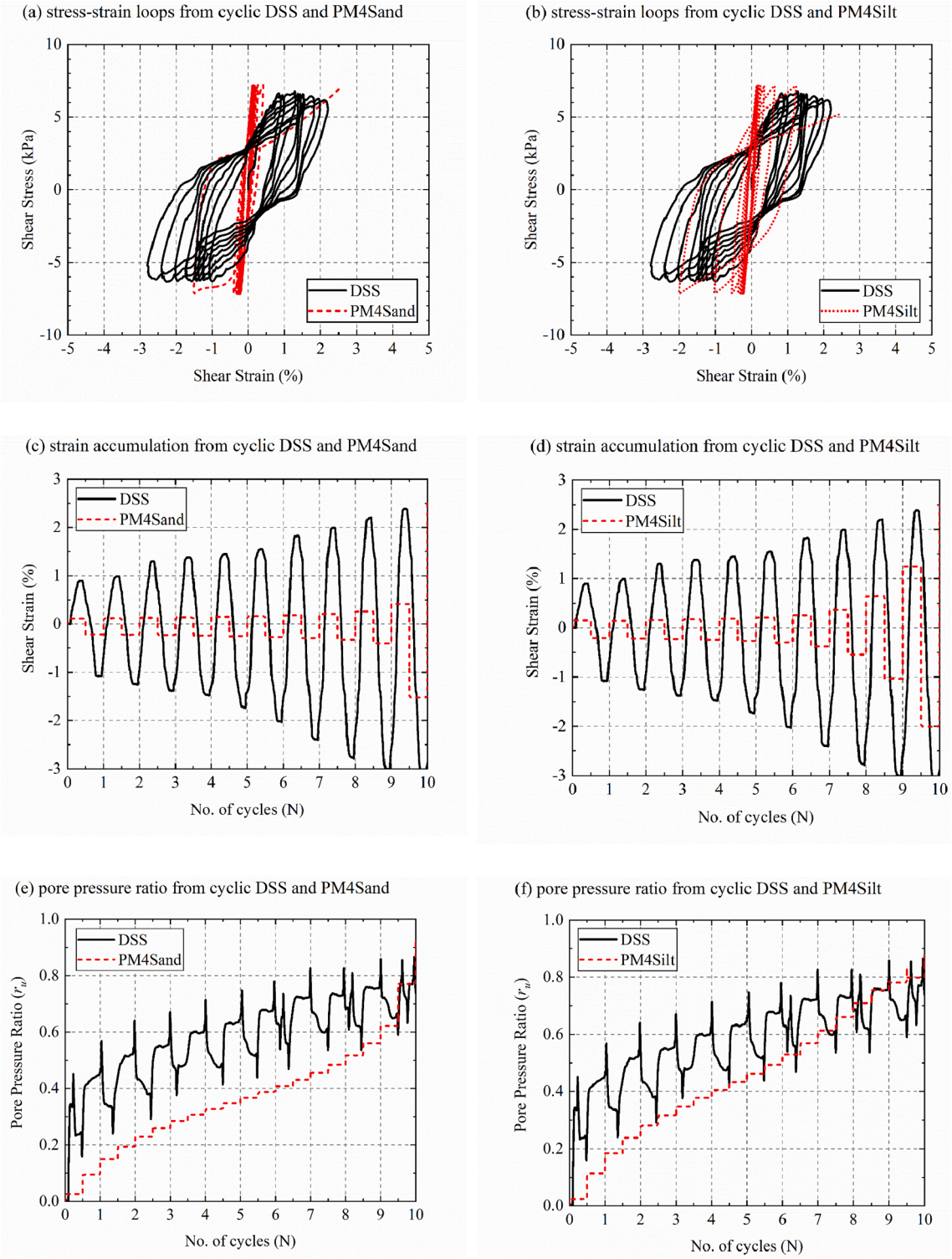


**Fig. 3.** Cyclic responses of CT from cyclic DSS test and simulations at CSR = 0.12.

may better represent the behavior and consistency of fine-grained material such as coal tailings compared to relative density ($D_r$ in PM4Sand). Therefore, PM4Silt was selected to model the CT in the seismic stability simulations.

### 2.2. Random fields generation for CT

Among the three primary input parameters ($s_{u,cs,eq\_Rat}$, $G_o$, and $h_{po}$) that are required to model the CT using PM4Silt, $s_{u,cs,eq\_Rat}$ was modeled as a spatially correlated Gaussian random field. Random field representation approach has been adopted in several other geotechnical engineering applications [e.g. Boulanger, 2019; Boulanger and Montgomery, 2016; Fenton and Griffiths, 2003]. Random fields are defined by a probability distribution, including mean and standard deviation, and auto-correlation functions based on available data. An auto-correlation function states the distance in vertical and horizontal directions, within which soil properties are correlated. The Karhunen-Loeve (K-L) expansion method was adopted to generate and discretize

the random fields, as described in Phoon and Ching (Phoon and Ching, 2014) and Eq. (1):

$$R(x,y,\theta) \approx \mu + \sum_{i=1}^{M} \sqrt{\lambda_i}\Phi_i(x,y)\xi_i(\theta) \quad (1)$$

$R(x,y,\theta)$ is the Gaussian random filed, where $x$ and $y$ are the coordinates of the points in the space, $\theta$ denotes the stochastic characteristic of the random field such that $\xi_i(\theta)$ are uncorrelated standard random variables with zero mean and unit standard deviation. $\lambda_i$ and $\Phi_i$ are the eigenvalues and eigenfunctions, respectively, of the covariance matrix formed by the covariance function (Eq. (2)). $M$ is the truncation order of the expansion series and determines the accuracy and smoothness of the generated random field. The series was truncated at $M = 10$, where sufficient accuracy and smoothness were achieved for the distribution of $s_{u,cs,eq\_Rat}$ within the random fields.

The undrained shear strength of tailings and similar soils such as silty alluvial soils reported in the literature (e.g. Castro, 2003, Hegazy et al., 2004, Idriss and Boulanger, 2008, Kalinski and Salehian, 2016, Ladd and Foott, 1974, Olson and Stark, 2002, Phoon et al., 1995, Phoon and Kulhawy, 1999, Robertson, 2009, Salam et al., 2019, Yu et al., 2019) were used to establish the probability distribution for $s_{u,cs,eq\_Rat}$. Lognormal distribution has been commonly assumed for undrained shear strength of fine-grained soils (Fenton and Griffiths, 2005; Wolff et al., 1996). Accordingly, a lognormal distribution with mean value ($\mu$) of 0.2 and coefficient of variation (COV) of 20% was found the best estimate for $s_{u,cs,eq\_Rat}$. An exponential autocorrelation function was also adopted for the CT properties, as shown in Eq. (2). The correlation between arbitrary points in the random field is defined by the standard deviation of the random field ($\sigma$) and autocorrelation lengths ($l_x$ and $l_y$). Due to the limited data concerning the stratification of tailings, the horizontal ($l_x$) and vertical ($l_y$) autocorrelation lengths were adopted from values reported for alluvial silty soils, which have similar deposition process and composition to CT. Accordingly, the horizontal and vertical autocorrelation lengths were assumed to be 15 m and 1.5 m, respectively (Ji et al., 2012).

$$C[(x_1,y_1),(x_2,y_2)] = \sigma^2 exp\left(-\frac{|x_1-x_2|}{l_x} - \frac{|y_1-y_2|}{l_y}\right) \quad (2)$$

The shear modulus coefficient, $G_o$, was correlated to $s_{u,cs,eq\_Rat}$ by the equation proposed by Dickenson (Dickenson, 1994) with a slight adjustment to represent the CT shear modulus, as shown in Eq. (3). The main equation was developed for cohesive soils in the San Francisco Bay Area with a constant factor equal to 23. However, the constant factor was scaled up to 28 to fit the available data for the shear modulus of the tested CT by Salam et al. (Salam et al., 2019).

$$G_{max} = \rho \cdot \left(28 \cdot \left(s_{u,cs,eq\_Rat} \cdot \sigma'_v\right)^{0.475}\right)^2 \quad (3)$$

where $\rho$ is total density and $\sigma'_v$ is vertical effective stress. Keeping $h_{po}$ constant (Boulanger and Montgomery, 2016), the CSR versus number of cycles to reach 5% DAS for the CT was simulated for three values of $s_{u,cs,eq\_Rat}$ (i.e. 0.15, 0.2, and 0.25) using PM4Silt. Fig. 4 shows the increasing trend in cyclic resistance of CT due to increase in $s_{u,cs,eq\_Rat}$. For example, the required number of cycles to reach 5% shear strain increased from approximately 8 to 25, when $s_{u,cs,eq\_Rat}$ of CT increased from 0.15 to 0.25. Fig. 4 signifies the necessity of sensitivity analysis and stochastic modeling for the seismic stability of CT dams.

In order to stochastically evaluate seismic stability of the model, 66 realizations for the CT section in the model were selected. The Latin Hypercube Sampling (LHS) method was adopted to select the representative realizations (Betz et al., 2014). Fig. 5 presents four realizations (A, B, C, and D) out of the 66 selected realizations. The $s_{u,cs,eq\_Rat}$ range varies among the realizations. For example, the maximum values for $s_{u,cs,eq\_Rat}$ are 0.25, 0.35, 0.5, and 0.3 in Realization A to D, respectively. As shown in Fig. 5, the variability of $s_{u,cs,eq\_Rat}$ forms extremely strong and weak

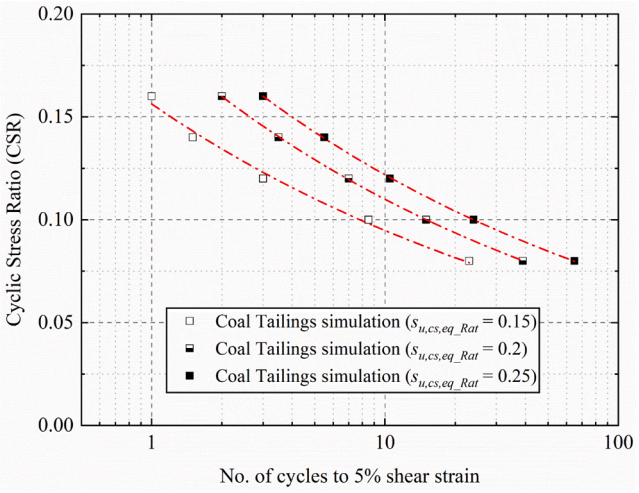


**Fig. 4.** CSR-N curves (PM4Silt simulation results).

pockets within the tailings, which could contribute to co-seismic or post-seismic failure of the CT dam. The $s_{u,cs,eq\_Rat}$ variation through depth and horizontal distance is also shown in Fig. 5. The solid line shows the average $s_{u,cs,eq\_Rat}$, which fluctuates around the set average value (i.e. 0.2) in both vertical and horizontal directions. Three uniform models were also generated with $s_{u,cs,eq\_Rat}$ of 0.15 (lower bound), 0.2 (best estimate), and 0.25 (upper bound). $s_{u,cs,eq\_Rat} = 0.15$ was selected to represent a weak CT dam; and $s_{u,cs,eq\_Rat} = 0.25$ was selected to represent a strong CT dam.

## 3. Input motions and analysis approach

Six input motions were selected to investigate the effect of PGA, ENC as a proxy for duration, and frequency content on seismic stability of the CT dam. Fig. 6 presents the acceleration time histories and the response spectra of the input motions. In order to investigate the effect of PGA, the 2011 Mineral Virginia Earthquake ($M_w = 5.8$), a shallow crustal event recorded at the Corbin station, was selected. The event was scaled to bedrock outcrop PGAs of 0.24 g, 0.37 g, and 0.5 g and referred to as EQ1, EQ2, and EQ3, respectively. The bracketed duration ($D_{5\text{-}95}$) of the Mineral Virginia Earthquake was approximately 20 s. Accordingly, to reduce the simulation cost, only 20 s of the motion, the significant duration, was used for the dynamic analysis. Accordingly, the bracketed duration ($D_{5\text{-}95}$) of the adopted motion was approximately 6.4 s. The response spectra of EQ1, EQ2, and EQ3 in Fig. 6 reflect the 20 s motion. A blast motion (provided by Vibra Tech, Inc., Hazleton, PA), as a common cyclic loading around mine sites and tailings dams, was adopted. The blast motion (denoted as B1) had a duration of 5 s and was scaled to an outcrop PGA of 0.24 g using a scaling factor equal to 4. Accordingly, the effect of frequency content and duration could be studied by comparing the system response under EQ1 and B1.

The 1940 El Centro Earthquake ($M_w = 6.9$) recorded at the El Centro Array 9 station and the 1992 Landers Earthquake ($M_w = 7.3$) recorded at the Yermo fire station both with scaled outcrop PGA of 0.24 g were selected and are referred to as EQ4 and EQ5, respectively. The scaling factors for these motions were 0.75 and 0.96. The bracketed duration of EQ4 and EQ5 was 24.3 s, and 18.9 s, respectively. The bracketed durations of the selected earthquakes are different, therefore, EQ4 and EQ5 impose larger number of cycles and more impact on the CT dam, as their durations are significantly longer. The effect of duration and frequency content could be studied by investigating the system response under EQ1, EQ4, and EQ5, which have the same PGA.

ENC was adopted as a proxy for duration in this study. The ENC of each input motion was determined according to the criteria discussed by Verma et al. (Verma et al., 2018). Non-linear dynamic analysis was performed for the uniform models to determine the peak ground

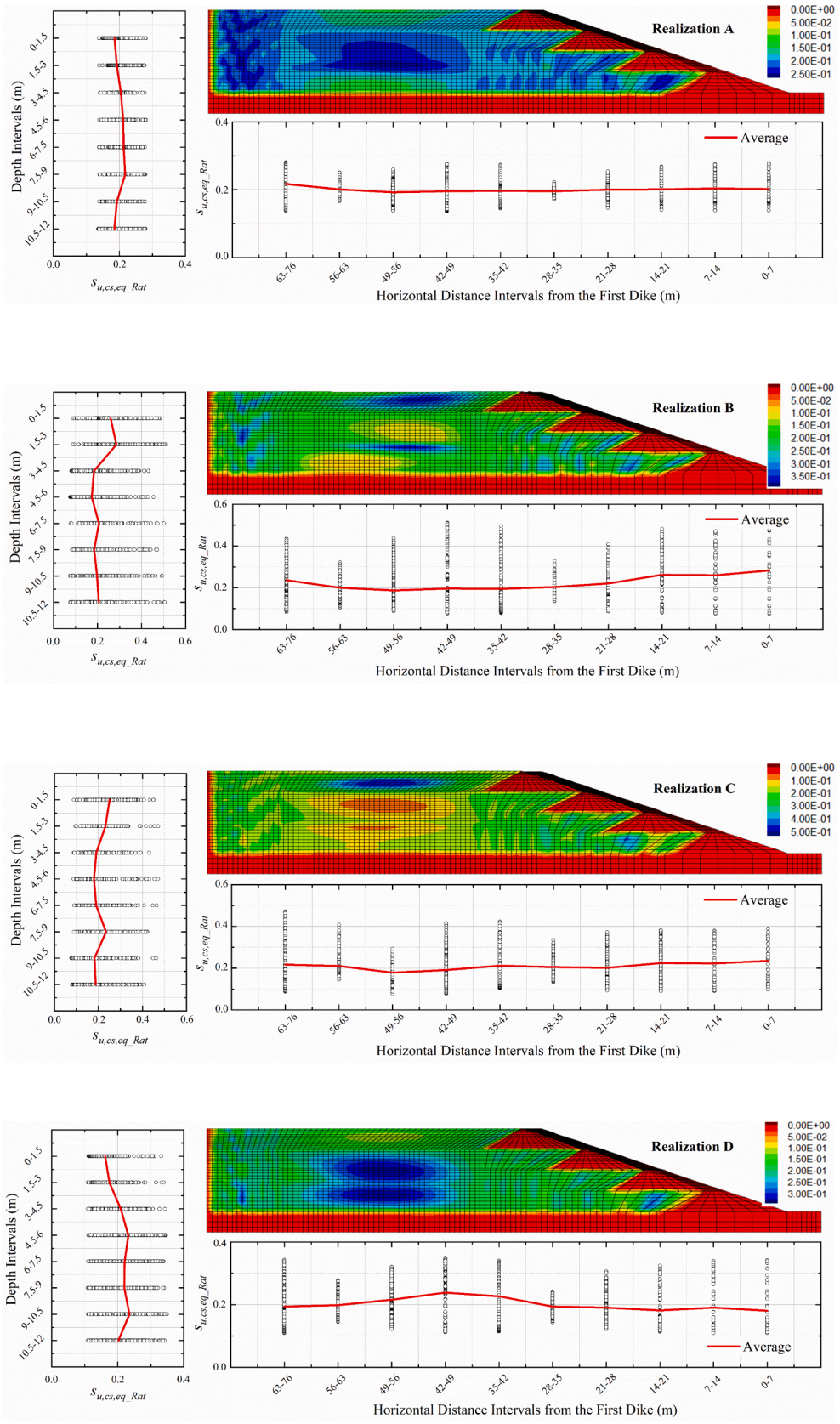


**Fig. 5.** $s_{u,cs,eq\_Rat}$ variation in Realizations A, B, C, and D.

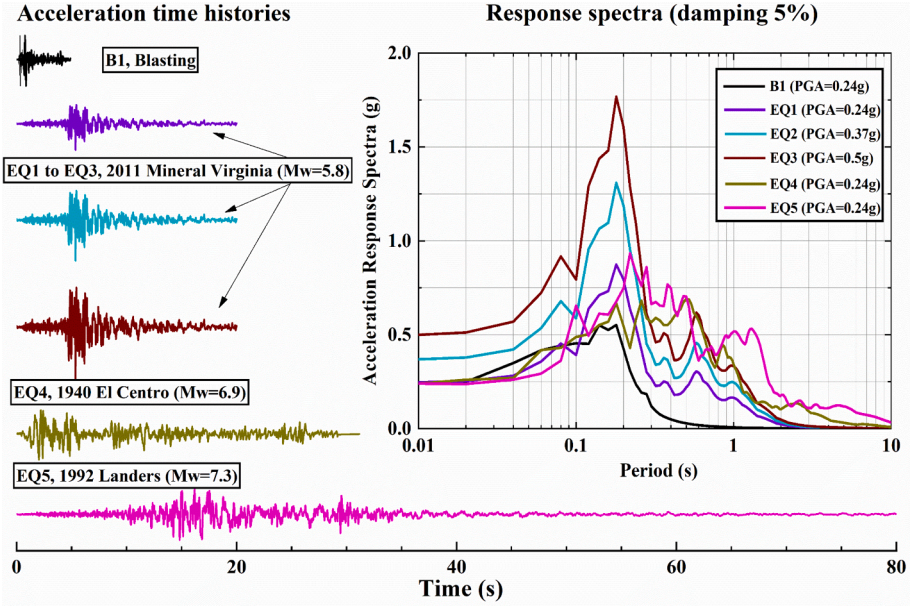


**Fig. 6.** Selected input motions for seismic stability analyses of CT dam.

acceleration at the ground surface. The maximum acceleration at the ground surface from the dynamic analysis was used as an approximate estimate of PGA in non-liquefied conditions as the input of the simplified triggering correlations by Seed and Idriss (Seed and Idriss, 1971). Fig. 7 presents the CSR and ENC of the selected input motions. The ENC of the input motions of EQ1, EQ2, EQ3 and B1 is approximately 11. The ENC of EQ4 and EQ5 is 30 and 38, respectively. The CSR-N curve of the tested CT sample is also shown in Fig. 7 as a reference. Since the constitutive model was calibrated to capture the cyclic DSS results, this figure implies that for all input motions in this study, the soil element is expected to liquefy. The dynamic response of the dam is more complex since liquefaction at deeper depths could change the propagation of motions throughout the soil profile and inevitably change the cyclic shear stress that the shallower soil elements are subjected to. The effective-stress dynamic 2D analysis that is presented in the next section enables us to look into the complex dynamic response of the dam subjected to soil liquefaction. As far as the frequency content effect, significant vibration and deformations are likely to occur when input motion and system response spectra are in tune with each other such that natural periods of the input motion are similar to those of the system.

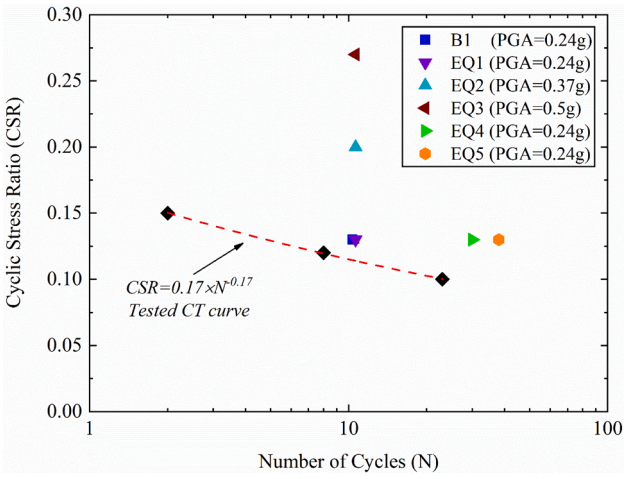


**Fig. 7.** ENC and maximum CSR of the input motions and CSR-N curve of the tested CT.

## 4. Model results and discussion

### 4.1. Representative dynamic responses

Figs. 8 and 9 show the co-seismic performance of the CT dam in terms of excess pore pressure and shear strain contours under the input motion EQ2, as an example. Fig. 8 shows the results of the uniform model with $s_{u,cs,eq\_Rat} = 0.2$, and Fig. 9 shows the results of the stochastic model with $s_{u,cs,eq\_Rat}$ ranging from 0.1 to 0.5. The maximum excess pore pressures generated during EQ2 were equal in both the uniform model and the stochastic model. However, in the stochastic model larger area in the vicinity of the dikes experienced high residual excess pore pressure. Generation of excess pore pressure leads to softening and consequently large deformation of the CT dam. Accordingly, although the shear band and deformation pattern were similar in Figs. 8 and 9, the maximum shear strain developed in the stochastic model was larger than that of the uniform model. In addition, the residual excess pore pressure may result in post-seismic failure, which is a common concern for CT dams. Accordingly, the larger area with high residual excess pore pressure in the stochastic model implied higher risk of post-seismic failure.

Fig. 10 shows the stress path and shear stress vs. shear strain evolutions under EQ2 at two locations selected from the uniform model with $s_{u,cs,eq\_Rat} = 0.2$ and a stochastic model with $s_{u,cs,eq\_Rat}$ varying from 0.1 to 0.3. The $s_{u,cs,eq\_Rat}$ of the uniform model was equal to 0.2 at both Locations 1 and 2, while the $s_{u,cs,eq\_Rat}$ of Location 1 and Location 2 in the stochastic model was 0.175 and 0.25, respectively, as shown in Fig. 10 (a). The effect of spatial variability on the shear mechanism in such complex system depends on the initial conditions such as effective stress, static shear stress ratio, and $s_{u,cs,eq\_Rat}$ in the stochastic model. In addition, the demand shear stress at such locations may significantly vary and be influenced by the response of the adjacent region during the dynamic loading. Therefore, the behavior and response at these locations are not as simple as a single element soil to interpret. Fig. 10 (b) and (c) show the shear stress vs. shear strain evolutions at Locations 1 and 2 in the stochastic and the uniform models, respectively. The shear strain remained positive and increased during the dynamic loading since the locations were close to the dikes. Location 1 showed 0.92% and 0.81% shear strain in the stochastic and the uniform model, respectively, as Location 1 had smaller $s_{u,cs,eq\_Rat}$, in the stochastic model. Location 2 showed 0.19% and 0.29% shear strain in the stochastic and the uniform

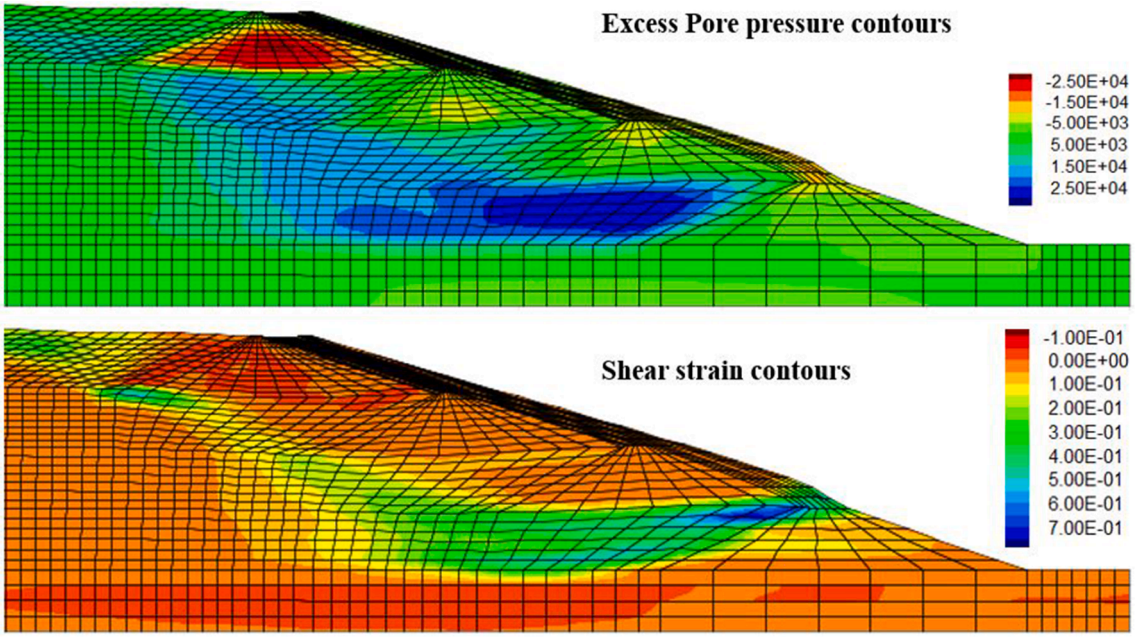


**Fig. 8.** Co-seismic performance of the CT dam in terms of excess pore pressure and shear strain contours in a uniform model with $s_{u,cs,eq\_Rat} = 0.2$ (The unit of excess pore pressure is Pa).

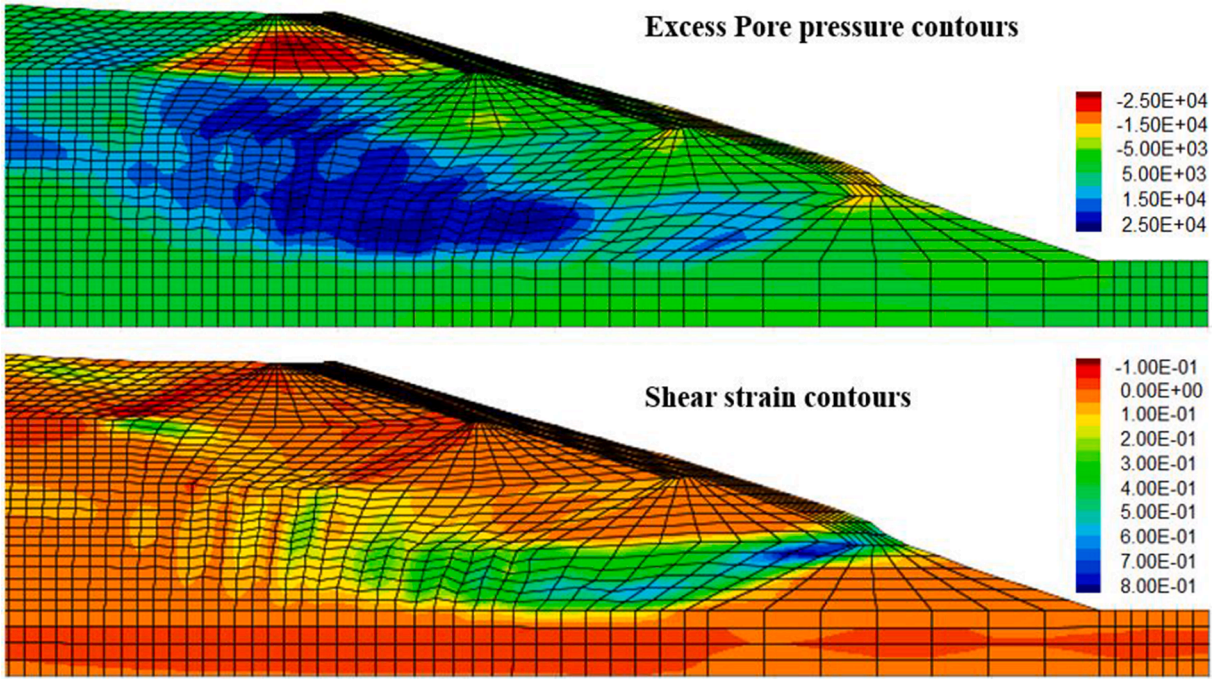


**Fig. 9.** Co-seismic performance of the CT dam in terms of excess pore pressure and shear strain contours in a stochastic model with $s_{u,cs,eq\_Rat}$ ranging from 0.1 to 0.5 (The unit of excess pore pressure is Pa).

model, respectively, as Location 2 had higher $s_{u,cs,eq\_Rat}$, in the stochastic model. According to Fig. 10 (b) to (e), larger shear strains associated with more reduction in the effective stress such as Location 1 in the stochastic model experienced approximately 30 kPa decrease in effective stress during the dynamic loading. Location 2 in the stochastic model only experienced 13 kPa reduction in effective stress. Location 1 and Location 2 in the uniform model experienced approximately 25 kPa and 23 kPa effective stress decrease, respectively.

Fig. 10 reveals that spatial variability causes variability in cyclic shear response within the system during the dynamic loading. This variability affects the shear wave propagation through the system, and it results in variability and uncertainty in the seismic stability of the CT dam. The significance and extent of these uncertainties are presented and discussed in the following sections.

### 4.2. Dynamic responses of uniform models

Fig. 11 presents the co-seismic and post-seismic crest settlements of the uniform models under the selected input motions except for B1. The CT dam was found to experience small crest settlement under B1 input

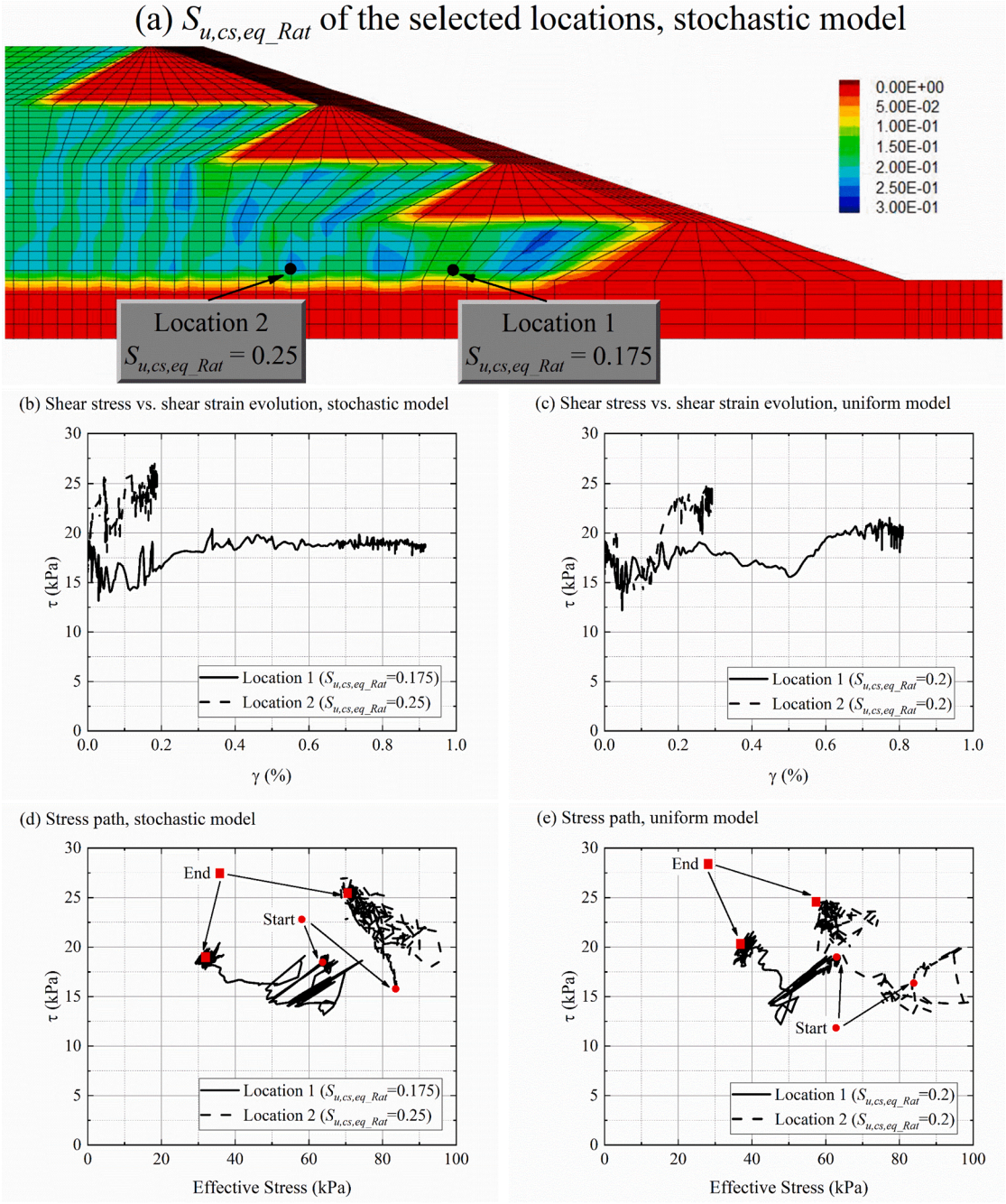


**Fig. 10.** Shear stress versus shear strain evolutions and stress path at two selected locations in CT under EQ2.

motion for both the stochastic and the uniform models, because of the short duration of the blast loading and the weak acceleration response spectra. The B1 input motion resulted in combined co-seismic and post-seismic crest settlement less than 0.05 m, which was significantly smaller than the crest settlements observed under the earthquake input motions. Therefore, the results of the blast input motion were excluded from further analyses.

In this study, complete failure was assumed if the crest settlement exceeded 3 m, which is equal to the height of a dike. Therefore, crest settlement larger than 3 m is not shown in Fig. 11. In general, the uniform models with higher $s_{u,cs,eq\_Rat}$ experienced smaller crest settlement. Fig. 11 (a) shows the effect of PGA (by comparing the results from EQ1 to EQ3) on the crest settlement of the uniform models. The uniform model with $s_{u,cs,eq\_Rat}$ of 0.25 showed the smallest crest settlement with post-seismic crest settlement less than 0.01 m. The co-seismic crest settlement increased from 0.281 m to 0.663 m when the PGA increased from 0.24 g to 0.5 g in the uniform model with $s_{u,cs,eq\_Rat}$ = 0.25. The uniform model with $s_{u,cs,eq\_Rat}$ = 0.2 experienced co-seismic crest settlement of 0.464 m, 0.946 m, 1.07 m under EQ1 to EQ3, respectively. The post-seismic crest settlement of the uniform model with $s_{u,cs,eq\_Rat}$ = 0.2 noticeably increased as PGA increased. The uniform model with $s_{u,cs,eq\_Rat}$ = 0.15 failed under EQ2 and EQ3. The co-seismic and post-seismic crest settlements of the uniform model with $s_{u,cs,eq\_Rat}$ = 0.15 under EQ1 were 0.75 m and 0.925 m, respectively.

Fig. 11 (b) shows the effects of ENC and frequency content on crest settlement. The increase of ENC from 11 to 38 (by comparing results from EQ1, EQ4, and EQ5) increased the crest settlement from 0.281 m to 1.03 m in the uniform models. The increasing trend in the crest settlement could also be due to richer response spectra of EQ4 and EQ5, which had higher acceleration in a wider range of periods compared to those of

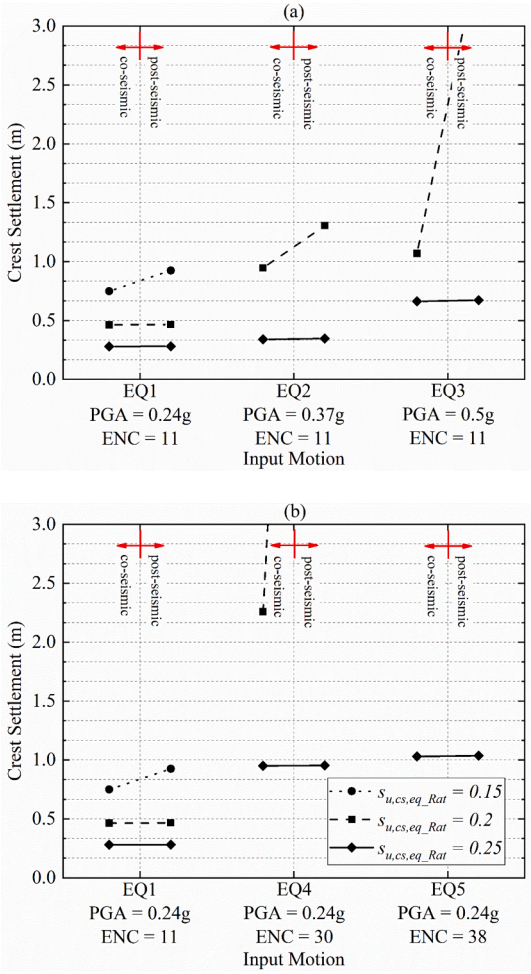


**Fig. 11.** Co-seismic and post-seismic crest settlements of the uniform models (a) PGA effect (b) ENC and frequency content effect.

EQ1. The post-seismic crest settlement of the uniform model with $s_{u,cs,eq\_Rat}$ = 0.25 was less than 0.01 m under EQ4 and EQ5. According to Fig. 11, significant additional settlement up to failure was observed for the uniform model with $s_{u,cs,eq\_Rat}$ = 0.2 during post-seismic analysis. The crest settlement of the uniform model with $s_{u,cs,eq\_Rat}$ = 0.2 exceeded 3 m (i.e. failure) during the post-seismic and co-seismic analysis of EQ4 and EQ5, respectively. The uniform model with $s_{u,cs,eq\_Rat}$ = 0.15 showed crest settlement beyond 3 m (i.e. failure) during co-seismic analysis under EQ4 and EQ5. Overall, the input motions with larger ENC and richer response spectra were found to cause larger crest settlement.

### 4.3. Significance of post-seismic analysis

The stochastic modeling revealed how the spatial variability of $s_{u,cs,eq\_Rat}$ within the CT section affects the co-seismic and post-seismic crest settlements. Fig. 12 demonstrates the co-seismic and post-seismic crest settlements under the input motion EQ2 for the uniform model with $s_{u,cs,eq\_Rat}$ = 0.2, Realizations A, B, C, D, and four other realizations (named E, F, G, and H). Fig. 12 shows the crest settlement of the uniform model with a solid line; the co-seismic and post-seismic crest settlements were 0.946 m and 1.306 m, respectively. The results of Realizations A to D are shown with dashed lines in Fig. 12. The extent of variability in both co-seismic and post-seismic settlements of the CT dam with spatially variable $s_{u,cs,eq\_Rat}$ can be seen in Fig. 12. While Realization B showed comparable crest settlement to the uniform model, Realizations A, C, and D had significantly different results. Realization C experienced small co-seismic and post-seismic crest settlements of 0.588 m and 0.671 m,

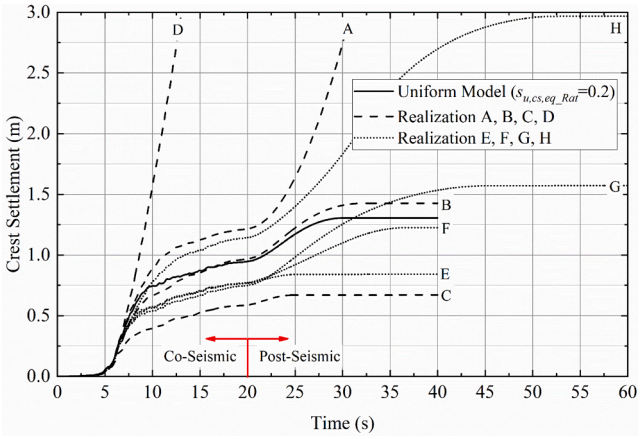


**Fig. 12.** Co-seismic and post-seismic performance of selected models under EQ2.

respectively. Realization A showed larger co-seismic crest settlement of 1.217 m and the CT dam failed during post-seismic analysis. Realization D was found to be the most vulnerable, as the failure occurred during co-seismic analysis.

The results of Realizations E to H, shown in dotted lines in Fig. 12, were included to demonstrate that the co-seismic performance alone may not accurately represent the dynamic deformations after cyclic loading. Therefore, post-seismic analysis is necessary in order to characterize the overall deformation of the CT dam. This finding is consistent with the findings of other studies using numerical simulations [e.g. Naesgaard and Byrne, 2007]. Realizations E, F, and G exhibited a co-seismic crest settlement of around 0.764 m, but the overall crest settlement ranged from 0.842 m to 1.570 m. In another example, although Realization H showed similar co-seismic crest settlement to that of Realization A, complete failure was not observed and the final crest settlement was 2.970 m in Realization H. Considering the variability presented in Fig. 12, co-seismic and post-seismic settlements of the CT dam are separately discussed under the input motions in Figs. 13 and 14.

### 4.4. Co-seismic response of stochastic models

The variation of the co-seismic crest settlement when CT properties are spatially variable is shown in Fig. 13. Fig. 13 includes two subfigures to separately present the influences of PGA, ENC and frequency content on the variation of the co-seismic crest settlement. The co-seismic crest settlements of the uniform models are also shown in Fig. 13. The normalized settlement (NS) is defined as the crest settlement divided by the dam's height (12 m). The realizations that resulted in complete failure (NS > 25%) are excluded from Fig. 13 to have better resolution for the rest of the realizations. Four levels of crest settlements were considered in this study to evaluate the performance of the CT dam subjected to liquefaction based on NS: stable (NS ≤ 5%), moderate damage (5% < NS ≤ 10%), severe damage (10% < NS ≤ 25%), and failure (NS > 25%). Fig. 13 also shows the percentages of the realizations in each category under each input motion.

As shown in Fig. 13 (a), the CT dam was found to be stable under EQ1 for all the realizations. EQ1 caused larger crest settlement (0.447 m on average) compared to that of B1 (below 0.050 m). The PGA and ENC of EQ1 and B1 were the same. Therefore, this observation could be mainly due to the richer acceleration response spectra of EQ1, which showed higher acceleration in a wider range of periods compared to B1. The majority of the realizations under EQ2 experienced moderate damage. EQ2 caused failure in 17% of the realizations and the crest settlements of the remaining realizations ranged from 0.588 m to 2.850 m. Approximately half of the realizations showed larger crest settlement than that

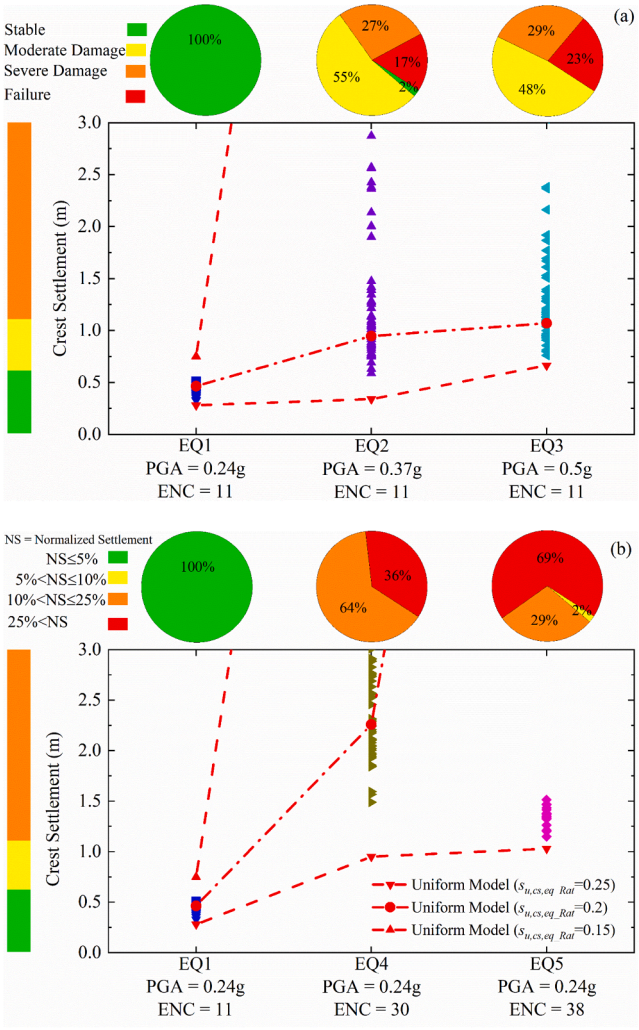


**Fig. 13.** Summary of co-seismic crest settlement for stochastic models (a) PGA effect (b) ENC and frequency content effect.

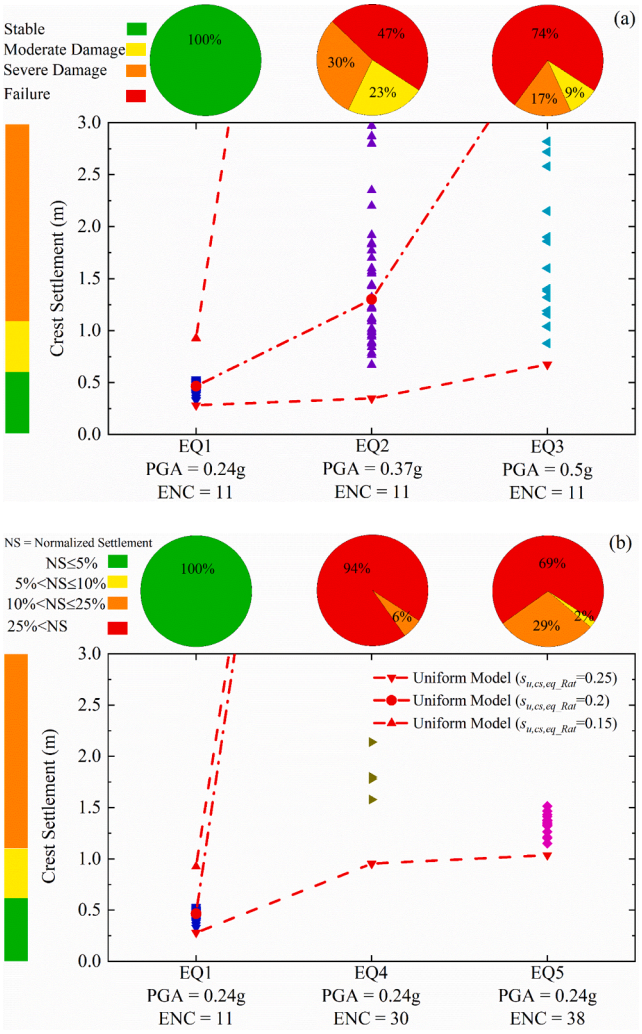


**Fig. 14.** Summary of post-seismic crest settlements for stochastic models (a) PGA effect (b) ENC and frequency content effect.

of the uniform model with $s_{u,cs,eq\_Rat} = 0.2$. The input motion EQ3 resulted in similar observations but more realizations (i.e. 23%) failed due to the higher PGA of this input motion. More than half of the realizations experienced larger crest settlement than that of the uniform model with $s_{u,cs,eq\_Rat} = 0.2$. Overall, increasing the PGA from 0.24 g to 0.5 g (i.e., from EQ1 to EQ3) increased failure probability. In addition, the discrepancy of the stochastic models' response from the response of the uniform model with $s_{u,cs,eq\_Rat} = 0.2$ became more significant as PGA increased. However, all the stochastic models' results were enveloped by the results of the uniform models with $s_{u,cs,eq\_Rat} = 0.15$ and $s_{u,cs,eq\_Rat} = 0.25$.

Fig. 13 (b) shows the effect of ENC and frequency content by comparing the results under EQ1, EQ4, and EQ5. EQ4 resulted in failure in 36% of the realizations, and the remaining experienced severe damage. More than half of the realizations showed crest settlement larger than that of the uniform model with $s_{u,cs,eq\_Rat} = 0.2$. EQ5, which had the largest ENC and magnitude among the input motions, caused failure in 69% of the realizations as well as failure in the uniform models with $s_{u,cs,eq\_Rat}$ of 0.2 and 0.15. However, 31% of the realizations under EQ5 showed NS $\leq$ 25% and experienced less crest settlement compared with EQ4. This could be attributed to the magnitude and frequency of the peaks in the acceleration spectra of EQ4 and EQ5 and their interaction with the natural frequencies of the stochastic models. This observation emphasized the necessity of stochastic modeling and frequency content analysis in seismic stability evaluation. The stochastic models' results were enveloped by the uniform models with $s_{u,cs,eq\_Rat}$ of 0.15 and 0.25.

### 4.5. Post-seismic response of stochastic models

Fig. 14 presents the final crest settlements after post-seismic analysis for the stochastic and the uniform models. The crest settlement that occurred during post-seismic analysis of EQ1 was negligible and less than 3% of the co-seismic crest settlement for both the stochastic and uniform models. As shown in Fig. 14 (a), the stochastic models showed additional settlement and higher probability of failure in post-seismic analysis. Under EQ2, approximately 75% of the realizations showed larger final crest settlement compared to that of the uniform model with $s_{u,cs,eq\_Rat} = 0.2$. Under EQ3, the uniform models with $s_{u,cs,eq\_Rat}$ of 0.2 to 0.15 and 74% of the realizations failed.

According to Fig. 14 (b), EQ4 was found to be the most destructive input motion among the input motions since 94% of the realizations failed. The higher failure rate observed for EQ4 compared to EQ5 after post-seismic analysis, despite the smaller ENC and magnitude of EQ4, could be attributed to the interplay between the system natural period and input motion acceleration spectra. Accordingly, the acceleration spectra of the input motion EQ4 were likely in tune with larger number of realizations and resulted in higher failure probability. This observation indicated the significance of all indices such that only one characteristic (e.g. ENC) may not be enough to predict the seismic performance of the CT dam.

### 4.6. Implications in practice

The significance of PGA, ENC, and frequency content in the seismic performance of the CT dam was assessed by paired *t*-test. The mean responses of the realizations under two input motions are compared in the paired *t*-test. For example, a statistically significant mean differences between EQ1 and EQ2, EQ1 and EQ3, EQ2 and EQ3 revealed the significance of PGA in the seismic performance of the CT dam. Conducting paired *t*-test on appropriate set of data, all the studied input motion characteristics (PGA, ENC, and frequency content) were found statistically significant.

To reveal the significant uncertainty and variation in seismic response due to spatial variability in $s_{u,cs,eq\_Rat}$, the one-sample *t*-test was adopted. This approach determines whether the average response (i.e. crest settlement) obtained from the stochastic models is significantly different from the crest settlement from the uniform model with $s_{u,cs,eq\_Rat} = 0.2$ (i.e. best estimate). This procedure was conducted for each earthquake input motion. The one-sample *t*-test was conducted once for co-seismic crest settlements and once for overall settlements (i.e. after post-seismic analysis). The one-sample *t*-test showed that the mean response of the stochastic models is statistically significantly different from the response of the uniform model with $s_{u,cs,eq\_Rat} = 0.2$ (i.e. best estimate), for both co-seismic and post-seismic settlements.

Therefore, the uniform model with best estimate ($s_{u,cs,eq\_Rat} = 0.2$) cannot properly capture the uncertainty in response caused by heterogeneity in subsurface condition. Furthermore, although the stochastic results were enveloped by the results of the uniform models with the lower bound ($s_{u,cs,eq\_Rat} = 0.15$) and the upper bound ($s_{u,cs,eq\_Rat} = 0.25$) properties, the probability of failure could not be estimated. For example, Fig. 13 (b) shows that the uniform model with lower bound properties ($s_{u,cs,eq\_Rat} = 0.15$) failed under EQ4, while the majority of the realizations (64%) did not experience failure. Therefore, uniform modeling may lead to conservative results. Stochastic modeling can be more efficient and used to perform a probabilistic analysis on seismic stability of CT dams.

## 5. Summary and conclusions

In this study, seismic stability of a typical upstream-construction CT dam was investigated considering the spatial variability in geotechnical properties of CT under six cyclic loadings. The cyclic behavior of CT was first approximated by PM4Sand and PM4Silt using the primary input parameters. PM4Silt was evaluated to better approximate the cyclic mobility and the progressive shear strain accumulation in CT under cyclic loading. Among the primary input parameters, the undrained shear strength ratio ($s_{u,cs,eq\_Rat}$) was modeled as a spatially correlated Gaussian random field. The effects of variability in CT's geotechnical properties and input motion characteristics (i.e. PGA, ENC, and frequency content) on the seismic stability of the CT dam were assessed. Uniform models with three different values, lower bound, best estimate, and upper bound for $s_{u,cs,eq\_Rat}$ were also studied under the selected input motions.

Among the uniform models, only the model with $s_{u,cs,eq\_Rat} = 0.2$ (i.e. best estimate) showed the necessity of post-seismic analysis, as the stability status changed during the post-seismic analysis. Post-seismic analysis was found critical for the stochastic models as failure probability significantly increased. The significance of stochastic modeling was statistically proved by comparing the results of the stochastic models and the uniform model with $s_{u,cs,eq\_Rat} = 0.2$ under the input motions. The discrepancy between stochastic and uniform modeling was intensified under stronger input motions. The majority of stochastic models experienced larger settlement than the uniform model with $s_{u,cs,eq\_Rat} = 0.2$. However, the range of stochastic results was captured by the uniform models with lower and upper bound values for $s_{u,cs,eq\_Rat}$ (i.e. 0.15 and 0.25).

This study highlighted the importance of stochastic modeling and the consideration of spatial variability in seismic stability analysis of CT dams. More investigations for different geometries, seismic demands, statistical characteristics of the random fields, and autocorrelation lengths are necessary, so that the findings of this study and the effects of PGA, ENC, frequency content, and other potential characteristics on the seismic response of CT dams can be further confirmed. Further case studies and in-situ data collection are needed to achieve improved insight into this topic such that the current uncertainties and drawbacks in calibration and spatial variability can be addressed.

## CRediT authorship contribution statement

**Sajjad Salam:** Conceptualization, Data curation, Formal analysis, Investigation, Methodology, Software, Validation, Visualization, Writing - original draft. **Ming Xiao:** Validation, Funding acquisition, Project administration, Resources, Supervision, Writing - review & editing. **Arash Khosravifar:** Data curation, Formal analysis, Validation, Methodology, Writing - review & editing. **Katerina Ziotopoulou:** Methodology, Supervision, Validation, Writing - review & editing.

## Declaration of Competing Interest

The authors declare that they have no known competing financial interests or personal relationships that could have appeared to influence the work reported in this paper.

## Acknowledgment

Authors would like to acknowledge the Itasca Consulting Group, Inc. for providing the license of FLAC through Itasca Education Partnership program.

## References

Azam, S., Li, Q., 2010. Tailings Dam Failures: A Review of the Last One Hundred Years. Geotech. News 28 (4), 50–54.

Beaty, M., Byrne, P. M., 1998. An Effective Stress Model for Predicting Liquefaction Behaviour of Sand. In: Geotechnical Earthquake Engineering and Soil Dynamics III, ASCE, pp. 766-777.

Betz, W., Papaioannou, I., Straub, D., 2014. Numerical Methods for the Discretization of Random Fields by Means of the Karhunen-Loève Expansion. Comput. Methods Appl. Mech. Eng. 271, 109–129.

Boulanger, R.W., 2019. Nonlinear Dynamic Analyses of Austrian Dam in the 1989 Loma Prieta Earthquake. J. Geotech. Geoenviron. Eng. 145 (11), 05019011.

Boulanger, R. W., Ziotopoulou, K., 2017. PM4Sand (Version 3.1): A Sand Plasticity Model for Earthquake Engineering Applications. Report No. UCD/CGM-17/01, Center for Geotechnical Modeling, Department of Civil and Environmental Engineering, University of California, Davis, CA, March, 114 pp.

Boulanger, R. W., Ziotopoulou, K., 2018. PM4Silt (Version 1): A Silt Plasticity Model for Earthquake Engineering Applications. Report No. UCD/CGM-18/01, Center for Geotechnical Modeling, Department of Civil and Environmental Engineering, University of California, Davis, CA.

Boulanger, R.W., Montgomery, J., 2016. Nonlinear Deformation Analyses of an Embankment Dam On A Spatially Variable Liquefiable Deposit. Soil Dyn. Earthquake Eng. 91, 222–233.

Boulanger, R.W., Munter, S.K., Krage, C.P., DeJong, J.T., 2019. Liquefaction Evaluation of Interbedded Soil Deposit: Çark Canal in 1999 M7. 5 Kocaeli Earthquake. J. Geotech. Geoenviron. Eng. 145 (9), 05019007.

Byrne, P. M., Seid-Karbasi, M., 2003. Seismic Stability of Impoundments. In Proceedings of the 17th Annual Symposium, Vancouver Geotechnical Society, Vancouver, BC.

Castillo, J., Hallman, D., Byrne, P., Parra, D., 2005. Dynamic Analysis of Heap Leach Pad under High Phreatic Levels. In Proceedings of 27th Mining convention, Arequipa, Peru.

Castro, G., 2003. Evaluation of Seismic Stability of Tailings Dams. In Proceedings of the 12th Pan-American Conference on Soil Mechanics and Geotechnical Engineering, Cambridge, MA, pp. 16-23.

Dafalias, Y.F., Manzari, M.T., 2004. Simple Plasticity Sand Model Accounting for Fabric Change Effects. J. Eng. Mech. 130 (6), 622–634.

Dickenson, S.E., 1994. Dynamic Response of Soft and Deep Cohesive Soils during the Loma Prieta Earthquake of October 17, 1989, PhD thesis, Dept. of Civil and Enviro. Eng., University of California, Berkeley, CA.

Fenton, G.A., Griffiths, D.V., 2003. Bearing-Capacity Prediction of Spatially Random C-Φ Soils. Can. Geotech. J. 40 (1), 54–65.

Fenton, G.A., Griffiths, D.V., 2005. Three-dimensional Probabilistic Foundation Settlement. J. Geotech. Geoenviron. Eng. 131 (2), 232–239.

Ferdosi, B., James, M., Aubertin, M., 2015. Effect of Waste Rock Inclusions on the Seismic Stability of an Upstream Raised Tailings Impoundment: A Numerical Investigation. Can. Geotech. J. 52 (12), 1930–1944.
Hardin, B.O., 1978, June. The nature of stress-strain behavior for soils. In From Volume I of Earthquake Engineering and Soil Dynamics–Proceedings of the ASCE Geotechnical Engineering Division Specialty Conference, June 19-21, 1978, Pasadena, California.
Hegazy, Y. A., Cushing, A. G., Lewis, C. J., 2004. Physical, Mechanical, and Hydraulic Properties of Coal Refuse for Slurry Impoundment Design. D'Appolonia Engineering.
Home, A., 2019. Brazilian Mine Tragedy Will Not Be the Last Tailings Dam Disaster: Andy Home, <https://www.reuters.com/article/us-vale-sa-disaster-ahome/brazilian-mine-tragedy-will-not-be-the-last-tailings-dam-disaster-andy-home-idUSKCN1Q405J>.
International Commission on Large Dams (ICOLD), 2001. Tailings Dams - Risk Of Dangerous Occurrences, Lessons Learnt from Practical Experiences (Bulletin 121). Paris: International Commission on Large Dams (ICOLD).
Idriss, I.M., Boulanger, R.W., 2008. Soil Liquefaction during Earthquakes. Earthquake Engineering Research Institute, Monograph MNO 12.
Itasca Consulting Group, 2017. Fast Lagrangian Analysis of Continua, Version 8.0.
James, M., 2009. The Use of Waste Rock Inclusions to Control the Effect of Liquefaction in Tailings Impoundments. Ph.D. Dissertation, Department of Civil, Geological, and Mining Engineering, Ecole Polytechnique de Montreal, Montréal, Quebec.
Ji, J., Liao, H.J., Low, B.K., 2012. Modeling 2-D Spatial Variation in Slope Reliability Analysis Using Interpolated Autocorrelations. Comput. Geotech. 40, 135–146.
Kalinski, M.E., Salehian, A., 2016. Estimating the Cyclic and Post-Earthquake Behavior of Coal Mine Tailings at a Site in Eastern Kentucky. Geo-Chicago 279–288.
Ladd, C.C., Foott, R., 1974. New Design Procedure for Stability of Soft Clays. J. Geotech. Geoenviron. Eng. 100(Proc Paper 10064).
Liew, M., Xiao, M., Liu, S., Rudenko, D., 2020. In Situ Seismic Investigations for Evaluating Geotechnical Properties and Liquefaction Potential of Fine Coal Tailings. J. Geotech. Geoenviron. Eng. 146 (5), 04020014.
Mejia, L. H., Dawson, E. M., 2006. Earthquake Deconvolution for FLAC. In FLAC and Numerical Modeling in Geomechanics. Proceedings of the 4th International FLAC Symposium, Madrid, Spain, pp. 211-219.
Naesgaard, E., Byrne, P. M., 2007. Flow liquefaction simulation using a combined effective stress–total stress model. In 60th. Canadian Geotechnical Conference, Canadian Geotechnical Society, Ottawa, Ontario.
Olson, S.M., Stark, T.D., 2002. Liquefied Strength Ratio from Liquefaction Flow Failure Case Histories. Can. Geotech. J. 39 (3), 629–647.
Phoon, K.K., Ching, J., 2014. Risk and Reliability in Geotechnical Engineering. CRC Press.
Phoon, K. K., Kulhawy, F. H., Grigoriu, M. D., 1995. Reliability-Based Design of Foundations for Transmission Line Structures. Rep. No. TR-105000, Electric Power Research Institute, Palo Alto, CA.
Phoon, K.K., Kulhawy, F.H., 1999. Characterization of Geotechnical Variability. Can. Geotech. J. 36 (4), 612–624.
Plant, K. F., Harriman, T., 2008. Root Cause Analysis of TVA Kingston Dredge Pond Failure on December 22, 2008 Volume I–Summary Report, Volume II–Geological and Field Explorations.
Rico, M., Benito, G., Diez-Herrero, A., 2008. Floods from Tailings Dam Failures. J. Hazard. Mater. 154 (1–3), 79–87.
Robertson, P.K., 2009. Evaluation of Flow Liquefaction and Liquefied Strength Using the Cone Penetration Test. J. Geotech. Geoenviron. Eng. 136 (6), 842–853.
Salam, S., Xiao, M., Khosravifar, A., Liew, M., Liu, S., Rostami, J., 2019. Characterizations of Static and Dynamic Geotechnical Properties and Behaviors of Fine Coal Refuse. Can. Geotech. J. 56 (12), 1901–1916.
Seed, H.B., Idriss, I.M., 1971. Simplified Procedure for Evaluating Soil Liquefaction Potential. J. Soil Mech. Found. Div.
Seid-Karbasi, M., Byrne, P.M., 2004. Embankment Dams and Earthquakes. Int. J. Hydropower Dams 11 (2), 96–102.
Verma, P., Seidalinova, A., Wijewickreme, D., 2018. Equivalent Number of Uniform Cycles versus Earthquake Magnitude Relationships for Fine-Grained Soils. Can. Geotech. J. 56 (11), 1596–1608.
Vick, S.G., 1990. Planning, Design, and Analysis of Tailings Dams. BiTech.
Wolff, T. F., Demsky, E. C., Schauer, J., Perry, E., 1996. Reliability Assessment of Dike and Levee Embankments. In Uncertainty in the Geologic Environment: From Theory to Practice (pp. 636-650). ASCE.
Yu, H., Zeng, X., Michael, P.R., 2019. Geotechnical Properties and Flow Behavior of Coal Refuse under Static and Impact Loading. J. Geotech. Geoenviron. Eng. 145 (7), 04019024.
Zeng, X., Goble, J. A., Fu, L., 2008. Dynamic Properties of Coal Waste Refuse in a Tailings Dam. In Geotechnical Earthquake Engineering and Soil Dynamics IV, pp. 1-14.
Ziotopoulou, K., Montgomery, J., 2017. Numerical Modeling of Earthquake-Induced Liquefaction Effects on Shallow Foundations. In Proceedings of the 16th World Conference on Earthquake Engineering, Paper, No. 2979, pp. 9-3.
Ziotopoulou, K., Boulanger, R.W., 2016. Plasticity Modeling of Liquefaction Effects under Sloping Ground and Irregular Cyclic Loading Conditions. Soil Dyn. Earthquake Eng. 84, 269–283.